JOURNAL OF GEOPHYSICAL RESEARCH, VOL. 94, NO. B2, PAGES 1765-1775, FEBRUARY 10, 1989

Role of Crustal Flexure in Initiation of Low-Angle Normal Faults and Implications For Structural Evolution of the Basin and Range Province

JON E. SPENCER

Arizona Geological Survey, Tucson

CLEMENT G. CHASE

Department of Geosciences, University of Arizona, Tucson

The mechanics of low-angle normal faulting has proved difficult to establish despite clear geological evidence for the existence of such faults. Gently dipping shear stress trajectories are necessary for nucleation and propagation of low-angle faults in a structurally isotropic medium. Such trajectories are not produced by simple horizontal extension, but do arise in the presence of flexural stresses. We model stress conditions in a cross section through the strong upper crust using Airy stress functions for a two-dimensional elastic medium. Numerical modeling indicates that high ratios of flexural stress to extensional stress produce conditions favorable for low-angle normal fault initiation at intermediate depths in an elastic medium. We propose that the gentle dip of Cenozoic low-angle normal faults in the Basin and Range Province resulted from flexural stresses that were produced by isostatically uncompensated surface and, especially, Moho relief. Resurgent mid-Cenozoic magmatism and the consequent reduction of the thermally dependent flexural strength of the mantle lithosphere transferred flexural stresses to the upper crust, causing or promoting initiation of low-angle normal faults. Temporal changes in structural style, from dominantly low-angle to dominantly high-angle normal faulting, may reflect reduction of the magnitude of flexural stresses in the upper crust due to flattening of the Moho and cooling of the mantle lithosphere.

INTRODUCTION

The very existence of low-angle normal faults, displacing thin, structurally disaggregated hanging-wall sheets that could only have been driven by gravity [e.g., *Compton et al.*, 1977; *Davis et al.*, 1980; *Spencer*, 1985], requires exceedingly low ratios of shear stress to normal stress during fault movement. On active faults, such low shear stress to normal stress ratios are indicated by the absence of detectable friction-generated heat [*Brune et al.*, 1969; *Lachenbruch and Sass*, 1980], low seismic moments [*Hanks*, 1977], and in situ stress measurements [*Zoback et al.*, 1987; *Mount and Suppe*, 1987]. In contrast, experimental rock mechanics data [*Byerlee*, 1978; *Brace and Kohlstedt*, 1980; *Kirby and Kronenberg*, 1987] and theoretical modeling of lithosphere flexure [*McNutt and Menard*, 1982; *De Rito et al.*, 1986] and of stresses needed to support topography [*Jeffreys*, 1976, p. 272] indicate that much higher shear stress to normal stress ratios are sustainable in the lithosphere. These apparently conflicting data are the basis of an important concept of lithospheric mechanics: shear stresses of much greater magnitude are needed for fault initiation than for movement on existent faults. Fault initiation does not apparently occur with a single seismic event, but requires numerous earthquakes to create a weak sheetlike inclusion within an otherwise strong medium [*Raleigh and Evernden*, 1981]. The tectonic setting and state of stress during fault initiation may thus be quite different than conditions during continued fault movement.

The strength of unsheared crustal rock is dependent on many variables, including temperature, lithostatic pressure, strain rate, mineralogy, and pore fluid pressure. Due to poor constraints on many of these variables, it is difficult to calculate strength as a function of depth, but in general the strongest zone in continental crust appears to be at a depth of approximately 8 to 15 km. This strong zone corresponds to the downward transition from brittle to ductile failure mechanisms, and is the region in which most large crustal earthquake hypocenters are located [e.g., *Sibson*, 1982; *Chen and Molnar*, 1983; *Jackson*, 1987]. The large deviatoric stresses sustainable by the strong brittle-ductile transition zone, in the absence of weak and favorably oriented shear zones, justify use of theories of elasticity in simulating possible stress conditions leading to fault initiation. Stresses leading to low-angle normal fault initiation must cause failure on gently dipping surfaces that cut, at a low angle, across this strong zone.

Cenozoic low-angle normal faults of large areal extent are widely recognized in the Basin and Range Province of western North America [e.g., *Crittenden et al.*, 1980; *Frost and Martin*, 1982]. The large areal extent of denuded footwalls, in the direction of displacement, of some of these faults argues against the interpretation that such faults formed with steep dips (60°-45°) and were rotated to gentle dips (20°-0°) during extensional tectonism. Such faults must have formed with gentle dips and are thus termed primary low-angle normal faults.

The shallow dip of primary low-angle normal faults indicates that the state of stress leading to fault initiation was not simply the result of a horizontal extensional stress superimposed on a structurally isotropic crust devoid of deviatoric stresses from other sources. Such a simple stress state should produce normal faults with dips of 60°. Additional stresses having other origins must have influenced the state of stress to produce low-angle normal faults. Application of a basal shear stress, in combination with horizontal compression, to an elastic medium yields stress conditions that could lead to normal failure on gently dipping surfaces [*Yin*, 1987]. Preliminary numerical approximations indicate that flexure also produces complex stress trajectory patterns that could possibly lead to low-angle normal fault initiation [*Spencer*, 1982]. In this study we use Airy stress functions to determine stress conditions resulting from application of a variety of boundary conditions to an elastic medium, and attempt to simulate conditions that might result in formation of primary low-angle normal faults. Our approach is similar to that of *Hafner* [1951], although we more thoroughly explore the effects of flexural stresses.

The general mechanics of flexure are illustrated by the

Paper number 88JB03742.
0148-0227/89/88JB-3742$05.00

mathematically simple case of a sinusoidally varying normal stress acting on the base or top of an elastic medium. Resultant stress trajectories suggest that low-angle normal faults would form if stress magnitudes are sufficiently large. Addition of horizontal extensional stress causes shear stress trajectories to steepen. Sinusoidal stress distributions can be added together in a Fourier series to model more complex boundary conditions that represent specific tectonic settings.

Isostatically uncompensated Moho and surface relief, originally produced by Mesozoic crustal shortening and supported by the flexural strength of the lithosphere, was possibly the most significant source of flexural stresses in the Basin and Range Province at the time of initial mid-Tertiary extension. Uncompensated surface and Moho relief would be expected in areas where the locus of surface uplift due to thrust faulting is laterally adjacent to the axis of kinematically linked, deep-seated crustal thickening. We model this tectonic setting using boundary conditions that simulate the flexurally supported, isostatically uncompensated loads, and calculate the resultant state of stress. We also model a solitary, short-wavelength, high-amplitude Moho bulge isostatically compensated by a long-wavelength, low-amplitude topographic load, with axes horizontally coincident. This setting is intended to represent the paired mountain range and Moho bulge mentioned above following erosional destruction of the mountain range.

We propose here that laterally varying, vertically directed normal stresses are a key element in modifying stress states to produce primary low-angle normal faults. Resultant bending stresses are predicted to produce complex stress trajectory orientations and stress magnitude distributions that include conditions favorable for low-angle normal fault initiation. We consider such stresses in the Basin and Range Province to have been fundamentally isostatic in nature, and to have originated primarily from isostatically uncompensated surface or Moho relief that was inherited from pre-mid-Tertiary compressional tectonism.

SIGNIFICANCE OF CORDILLERAN METAMORPHIC CORE COMPLEXES

Rocks that were within or below the brittle-ductile transition during mid-Cenozoic time have been exhumed by Cenozoic low-angle normal faulting in western North America and are exposed within Cordilleran metamorphic core complexes [*Crittenden et al.*, 1980]. Gently dipping mylonitic fabrics that formed under ductile conditions were overprinted by brittle deformation at progressively lower temperatures, and are exposed in the footwalls of large-displacement, low-angle normal faults known as detachment faults. In any given area, these footwall rocks were sequentially mylonitized, brittlely deformed, and exhumed during a single pulse of extensional deformation. The lateral (and initially downward) transition from nonmylonitic to mylonitic footwall rocks in metamorphic core complexes records the location of the brittle-ductile transition during initial low-angle extensional tectonism [*Wernicke*, 1981; *Davis*, 1983; *Reynolds*, 1985; *Davis et al.*, 1986].

The initial dip of detachment faults and their downdip continuations as ductile shear zones are debated topics. One view is that such brittle-ductile shear zones formed with a steep dip and were rotated along with footwall and hanging-wall blocks to gentle dips [e.g., *Davis*, 1983]. If rotation occurred in part by movement on younger, steeper normal faults, this view is consistent with the absence of first-motion fault plane solutions indicating seismic slip on faults with dips less than 30° [*Jackson*, 1987]. In contrast, the lateral extent, in the direction of extension, of exposed footwall rocks in some metamorphic core complexes is so great that significant rotation about a horizontal axis is precluded. For example, in the Harcuvar Mountains of west-central Arizona, largely nonmylonitic footwall rocks are exposed in a structurally continuous block for over 50 km in a direction perpendicular to the presumed axis of footwall rotation [*Reynolds and Spencer*, 1985]. In the adjacent Buckskin Mountains, the footwall of the Buckskin-Rawhide detachment fault is exposed continuously for 42 km in the direction of extension. Mylonitic footwall rocks in the Buckskin and Rawhide mountains vary only slightly in texture and composition across the entire breadth of the complex, indicating that initial footwall depths did not vary significantly from one end of the range to the other [*Rehrig and Reynolds*, 1980; *Bryant*, 1988; *Spencer and Reynolds*, 1988]. Seismic reflection profiling has also demonstrated the great lateral extent of detachment faults in the direction of fault displacement [*Allmendinger et al.*, 1983; *Frost and Okaya*, 1986]. Large-displacement, low-angle, normal shear zones certainly underwent some rotation and warping during tectonic denudation [e.g., *Howard et al.*, 1982; *Spencer*, 1984; *John*, 1987], but large-magnitude footwall rotations (greater than 30°–40°) during extensional tectonism would have uncovered Cenozoic granulites or even mantle peridotites, neither of which have been recognized in Cordilleran metamorphic core complexes. Available geologic and geophysical evidence thus supports the view that, in some areas, large-displacement low-angle shear zones formed at a low angle and cut across the strong brittle-ductile transition zone where brittle faults were initially gradational downdip into ductile shear zones.

The magnitude of uplift of footwall rocks in many Cordilleran metamorphic core complexes, during and following tectonic denudation, is larger than would be expected for simple tectonic denudation. Sedimentary basin formation is an expected result of large displacement on low-angle normal faults. In contrast, mylonitic and nonmylonitic footwall rocks rose to elevations where they were a source of coarse clastic debris shed into syntectonic extensional sedimentary basins [*Spencer*, 1984; *Miller and John*, 1988; *Spencer and Reynolds*, 1988], and some metamorphic core complexes are now elevated 1000-2000 m above surrounding areas. The large magnitude of isostatic uplift experienced by Cordilleran metamorphic core complexes is supportive of the hypothesis that local, downward projecting bulges on the Moho, not initially isostatically compensated by surficial relief, were the driving force behind uplift [*Holt et al.*, 1986] and that such bulges could have produced substantial flexural stresses prior to uplift.

NUMERICAL SIMULATION

Our approach has been to model the strong upper crust as a purely elastic, two-dimensional medium. Equations that satisfy various boundary conditions were used to generate stress trajectory diagrams and shear stress magnitude contour diagrams. These diagrams are considered to give reasonable approximations of the state of stress in the upper crust at low shear stress magnitudes, and of the strong zone enclosing the brittle-ductile transition at higher stress magnitudes.

Consider a function $\phi = f(x, y)$, where x and y are horizontal and vertical coordinates, respectively, that defines the state of stress in an elastic, two-dimensional rectangular medium with body forces absent or constant. If such a function satisfies the biharmonic equation

$$\frac{\partial^4 \phi}{\partial x^4} + 2\left[\frac{\partial^4 \phi}{\partial x^2 \partial y^2}\right] + \frac{\partial^4 \phi}{\partial y^4} = 0 \qquad (1)$$

then it satisfies the requirement of static equilibrium (external forces on the system must be balanced), the condition that externally applied boundary forces are in equilibrium with internal stresses, and the condition of compatibility which insures the appropriate relationships between the strain components [e.g., *Timoshenko and Goodier*, 1970, pp. 26–32].

The stress components may be found from the partial derivatives

$$\sigma_x = \frac{\partial^2\phi}{\partial y^2} - \rho g y \qquad \sigma_y = \frac{\partial^2\phi}{\partial x^2} - \rho g y \qquad \tau_{xy} = -\frac{\partial^2\phi}{\partial x \partial y} \tag{2}$$

where ρ is rock density and g is the acceleration of gravity. A function ϕ that satisfies (1) and the appropriate boundary conditions is known as a stress function or Airy stress function. Stress components (2) determined from different stress functions and representing different boundary conditions may be added together to model complex stress states.

Use of the $\rho g y$ term for calculation of σ_x in (2) is appropriate for an isotropic, lithostatic state of stress. We model an isotropic stress state as our initial condition, with deviatoric stresses resulting only from applied stresses at the boundaries. In this case, the $\rho g y$ terms in (2) can be ignored because they have no influence on the orientations and magnitudes of shear stresses.

End Normal Stress

The second-order polynomial

$$\phi_1 = \frac{a_1}{2}x^2 + b_1 xy + \frac{c_1}{2}y^2 \tag{3}$$

is a stress function that can be used to model a normal stress of magnitude N acting on the ends of a horizontal, rectangular cross section of length L and depth D. Boundary conditions are that the Earth's surface is stress free,

$$\sigma_y(x, 0) = \tau_{xy}(x, 0) = 0 \tag{4}$$

and that the end normal stress N does not vary with depth,

$$\sigma_x(0, y) = \sigma_x(L, y) = N \tag{5}$$

From (2) we find that

$$\sigma_x = c_1 \qquad \sigma_y = a_1 \qquad \tau_{xy} = -b_1$$

To satisfy (4), a_1 must equal zero, and to satisfy (4) and (5), b_1 must equal zero. Constant c_1 is simply equal to the applied end normal stress N. Thus for an end normal stress of magnitude N, the stress components are

$$\sigma_{x_1} = N \qquad \sigma_{y_1} = 0 \qquad \tau_{xy_1} = 0 \tag{7}$$

Basal Shear Stress

The third-order polynomial

$$\phi_2 = \frac{a_2}{6}x^3 + \frac{b_2}{2}x^2 y + \frac{c_2}{2}xy^2 + \frac{d_2}{6}y^3 \tag{8}$$

is used to model a basal shear stress of magnitude S represented by the boundary condition

$$\tau_{xy}(x, D) = S \tag{9}$$

Application of (2) to (8) yields

$$\sigma_x = c_2 x + d_2 y \tag{10}$$

$$\sigma_y = a_2 x + b_2 y \tag{11}$$

$$\tau_{xy} = -b_2 x - c_2 y \tag{12}$$

Consideration of (4), which is applicable here, indicates that $a_2 = 0$ in (11) and $b_2 = 0$ in (12). Consideration of (9) indicates that $c_2 = -S/D$ in (12) (given that $b_2 = 0$). Values can be assigned to d_2 to represent the horizontal component of a lithostatic stress (for the case of no deviatoric stress due to lithostatic load), and to represent additional horizontal stresses that increase linearly with depth [*Hafner*, 1951; *Yin*, 1987]. We use (3) to model horizontal stresses, and use the $\rho g y$ terms in (2) to model isotropic body forces; therefore we set $d_2 = 0$. Thus for a basal shear stress of magnitude S, the stress components are

$$\begin{aligned} \sigma_{x_2} &= (-S/D)x \\ \sigma_{y_2} &= 0 \\ \tau_{xy_2} &= (S/D)y \end{aligned} \tag{13}$$

Base Normal Stress

Equation (1) is satisfied by a stress function that varies sinusoidally with x and is otherwise a function of y only:

$$\phi_3 = \sin\frac{m\pi x}{L} f(y) \tag{14}$$

where m is an integer. Following *Timoshenko and Goodier* [1970, pp. 53-55], we let $m\pi/L = a$, substitute (14) in (1), and take the general integral of the resultant linear differential equation which yields the stress function

$$\phi_3 = \sin \alpha x\,(C_1 \cosh \alpha y + C_2 \sinh \alpha y + C_3 y \cosh \alpha y + C_4 y \sinh \alpha y) \tag{15}$$

and the corresponding stress components

$$\sigma_x = \frac{\partial^2\phi}{\partial y^2} = \sin \alpha x\,[C_1\alpha^2 \cosh \alpha y + C_2\alpha^2 \sinh \alpha y + C_3\alpha(2 \sinh \alpha y + \alpha y \cosh \alpha y) + C_4\alpha(2 \cosh \alpha y + \alpha y \sinh \alpha y)] \tag{16}$$

$$\sigma_y = \frac{\partial^2\phi}{\partial x^2} = -\alpha^2 \sin \alpha x\,(C_1 \cosh \alpha y + C_2 \sinh \alpha y + C_3 y \cosh \alpha y + C_4 y \sinh \alpha y) \tag{17}$$

$$\tau_{xy} = -\frac{\partial^2\phi}{\partial x \partial y} = -\alpha \cos \alpha x\,[C_1\alpha \sinh \alpha y + C_2\alpha \cosh \alpha y + C_3(\cosh \alpha y + \alpha y \sinh \alpha y) + C_4(\sinh \alpha y + \alpha y \cosh \alpha y)] \tag{18}$$

Unlike stress functions ϕ_1 and ϕ_2, stress function ϕ_3 is applicable where $y = 0$ at the middle, rather than the top, of the rectangular cross section. Boundary conditions at the upper and lower boundaries ($y = \pm c$) are

$$y = +c \qquad \tau_{xy} = 0 \qquad \sigma_y = -B \sin \alpha x \tag{19}$$

$$y = -c \qquad \tau_{xy} = 0 \qquad \sigma_y = -A \sin \alpha x \tag{20}$$

where A and B are the maximum normal stresses at the upper and lower surfaces, respectively, of the cross section (negative for compression).

Substituting (19) and (20) in (18) allows determination of relationships between constants

$$C_3 = -C_2\left[\frac{\alpha \cosh \alpha c}{\cosh \alpha c + \alpha c \sinh \alpha c}\right] \tag{21}$$

$$C_4 = -C_1\left[\frac{\alpha \sinh \alpha c}{\sinh \alpha c + \alpha c \cosh \alpha c}\right] \tag{22}$$

Using (19) and (20) in (17), adding and subtracting these equations, and using (21) and (22), we find

$$C_1 = \left[\frac{A + B}{\alpha^2}\right]\left[\frac{\sinh \alpha c + \alpha c \cosh \alpha c}{\sinh 2\alpha c + 2\alpha c}\right]$$

$$C_2 = -\left[\frac{A - B}{\alpha^2}\right]\left[\frac{\cosh \alpha c + \alpha c \sinh \alpha c}{\sinh 2\alpha c - 2\alpha c}\right]$$

$$C_3 = \left[\frac{A - B}{\alpha^2}\right]\left[\frac{\alpha \cosh \alpha c}{\sinh 2\alpha c - 2\alpha c}\right] \quad (23)$$

$$C_4 = -\left[\frac{A + B}{\alpha^2}\right]\left[\frac{\alpha \sinh \alpha c}{\sinh 2\alpha c + 2\alpha c}\right]$$

Substituting (23) in (16), (17), and (18) yields the stress components

$$\sigma_{x_3} = (A + B)\left[\frac{(\alpha c \cosh \alpha c - \sinh \alpha c)\cosh \alpha y}{\sinh 2\alpha c + 2\alpha c} - \frac{\alpha y \sinh \alpha y \sinh \alpha c}{\sinh 2\alpha c + 2\alpha c}\right]\sin \alpha x$$
$$- (A - B)\left[\frac{(\alpha c \sinh \alpha c - \cosh \alpha c)\sinh \alpha y}{\sinh 2\alpha c - 2\alpha c} - \frac{\alpha y \cosh \alpha y \cosh \alpha c}{\sinh 2\alpha c - 2\alpha c}\right]\sin \alpha x$$

$$\sigma_{y_3} = -(A + B)\left[\frac{(\alpha c \cosh \alpha c + \sinh \alpha c)\cosh \alpha y}{\sinh 2\alpha c + 2\alpha c} - \frac{\alpha y \sinh \alpha y \sinh \alpha c}{\sinh 2\alpha c + 2\alpha c}\right]\sin \alpha x$$
$$+ (A - B)\left[\frac{(\alpha c \sinh \alpha c + \cosh \alpha c)\sinh \alpha y}{\sinh 2\alpha c - 2\alpha c} - \frac{\alpha y \cosh \alpha y \cosh \alpha c}{\sinh 2\alpha c - 2\alpha c}\right]\sin \alpha x \quad (24)$$

$$\tau_{xy_3} = -(A + B)\left[\frac{\alpha c \cosh \alpha c \sinh \alpha y}{\sinh 2\alpha c + 2\alpha c} - \frac{\alpha y \cosh \alpha y \sinh \alpha c}{\sinh 2\alpha c + 2\alpha c}\right]\cos \alpha x$$
$$+ (A - B)\left[\frac{\alpha c \sinh \alpha c \cosh \alpha y}{\sinh 2\alpha c - 2\alpha c} - \frac{\alpha y \sinh \alpha y \cosh \alpha c}{\sinh 2\alpha c - 2\alpha c}\right]\cos \alpha x$$

Stress functions of this form (14) representing different frequencies m and amplitudes A and B can be added together in a Fourier series to model a variety of normal stress distributions at the upper and lower surfaces. In this case,

$$\sigma_{x_3} = \sum_{i=1}^{n} \sigma_{x_{3_i}} \qquad \sigma_{y_3} = \sum_{i=1}^{n} \sigma_{y_{3_i}} \qquad \tau_{xy_3} = \sum_{i=1}^{n} \tau_{xy_{3_i}} \quad (25)$$

where n is the number of Fourier coefficients. The Fourier coefficient for the laterally invariant normal stress was set at zero as it does not satisfy (14).

Composite Stress States

Stress components determined for each of a number of boundary conditions can be added to yield a composite stress state. In our numerical simulations we consider only the three types of externally applied stresses described above. Resultant composite stress components from (7), (13), and (25) are

$$\sigma_x = N - Sx/D + \sum_{i=1}^{n} \sigma_{x_{3_i}} \qquad \sigma_y = \sum_{i=1}^{n} \sigma_{y_{3_i}}$$

$$\tau_{xy} = Sy/D + \sum_{i=1}^{n} \tau_{xy_{3_i}} \quad (26)$$

The orientation θ with respect to the x axis (moving anticlockwise from the x axis) of the least compressive principal stress is

$$\theta = 0.5 \arctan (2\tau_{xy}/(\sigma_x - \sigma_y)) \quad (27)$$

The greatest principal compressive stress is oriented at 90° to θ, and the predicted surfaces of failure, using simple Mohr-Coulomb failure criteria, are disposed at 30° about the greatest compressive principal stress. Principal stress trajectories, and shear stress trajectories representing the predicted surfaces of failure, were calculated from (26) and (27) and plotted using a microcomputer.

DISCUSSION OF RESULTS

The orientations of stress trajectories for each of the three types of boundary condition outlined above are independent of the magnitude of the applied stresses. The orientations vary greatly with different ratios of the applied stress magnitudes where boundary conditions are combined to yield composite stress states. Different ratios of boundary stress magnitudes can be plotted in Figure 1. Principal stress trajectories for each type of boundary stress corresponding to the corners of the diagram in Figure 1 are shown in Figure 2. In this study we explore

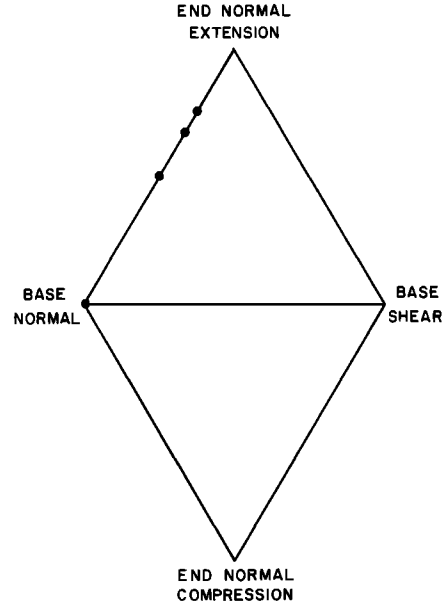

Fig. 1. Diagram representing range of possible combinations of boundary stress conditions for which numerical approximation methods are presented here. Dots along upper left edge represent states of stress modeled in Figure 3.

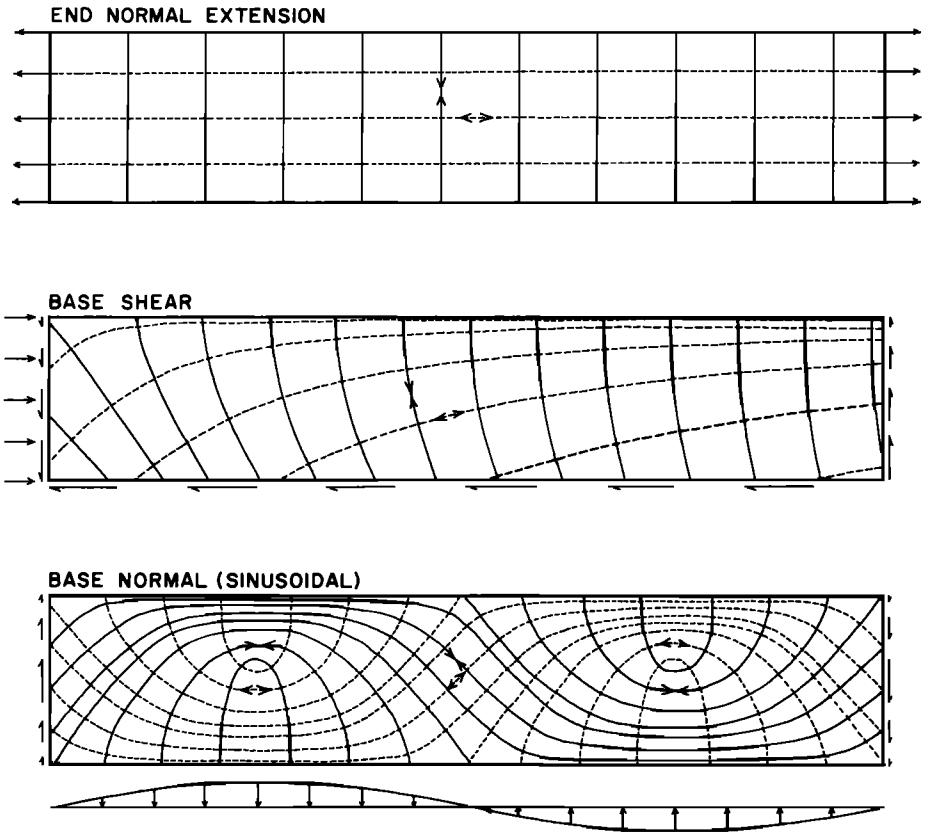

Fig. 2. Principal stress trajectories for end-member stress states represented by the corners of the upper triangle in Figure 1.

states of stress produced by different ratios of end normal extensional stress and laterally varying base and top normal stress, with no basal shear stress. These states of stress are represented by the upper left edge of the stress ratio diagram in Figure 1.

The upper right and lower right edges of Figure 1, representing varying ratios of end normal and base shear stress, were explored by *Yin* [1987], who determined that end normal compression combined with basal shear produces states of stress appropriate for low-angle normal fault initiation (lower right edge in Figure 1). Although *Yin* [1987] used constant d_2 in (8) to simulate downward increasing end normal stresses, in contrast to our modeling of an end normal stress that is constant with depth, stress trajectory orientations are not significantly different for the two approaches.

Sinusoidal Base Normal Stress

Predicted failure-surface trajectories oriented at 30° to the greatest compressive principal stress are shown in Figure 3 for four different ratios of end normal to sinusoidally varying base normal stress. The lowermost cross section shows failure-surface trajectories where end normal stresses are nonexistent. A contour diagram of shear stress magnitudes for this cross section is shown in Figure 4. Shear stress magnitude drops to zero at points located at depths of slightly less than one half the thickness of the cross section and directly above the points of maximum applied base normal stress, which correspond to the crests and troughs of the sine function representing the magnitude of the basal normal stress. These points of zero shear stress correspond to the intersection of the neutral surface with the axial planes of antiforms and synforms that would form as a consequence of the applied stresses. Shear stress magnitude increases above and below the points of zero shear stress, reaching maximums at the upper and lower edges of the cross section. Principal stresses are vertical and horizontal along the axial planes (Figure 2), and reverse or high-angle normal faulting would be predicted to occur near the edges of the cross section in the regions above and below the points of zero shear stress.

Above the points of zero base normal stress, which correspond to the inflection points in the sine function representing the basal stress magnitude, shear stress magnitude is zero at the upper and lower edge of the cross section, and reaches a maximum near the middle (Figure 4). Figure 4 and the lowermost cross section in Figure 3 indicate clearly that, if bending stresses alone are sufficient to cause failure at intermediate depths in an otherwise elastic medium, they will do so near the midpoint between the points of zero shear stress, and failure surfaces will dip approximately 15° (normal slip) or 75° (reverse slip).

Increased horizontal extensional stress causes the intermediate-depth points of zero shear stress to migrate toward the upper and lower edges, and results in steepening of the gently dipping failure-surface trajectories. At ratios of end normal extensional stress to maximum base normal stress approaching 3:1 (uppermost cross section in Figure 3) almost all failure surfaces dip at least 40° and have a normal sense of shear. At constant bending stress, increased horizontal extensional stress causes a simultaneous increase in the dip of initially gently dipping potential-failure surfaces and in the shear stress magnitude in the intermediate-depth, high-stress areas (Figure 5). This indicates that if bending stresses are insufficient to cause failure at intermediate depths, increased

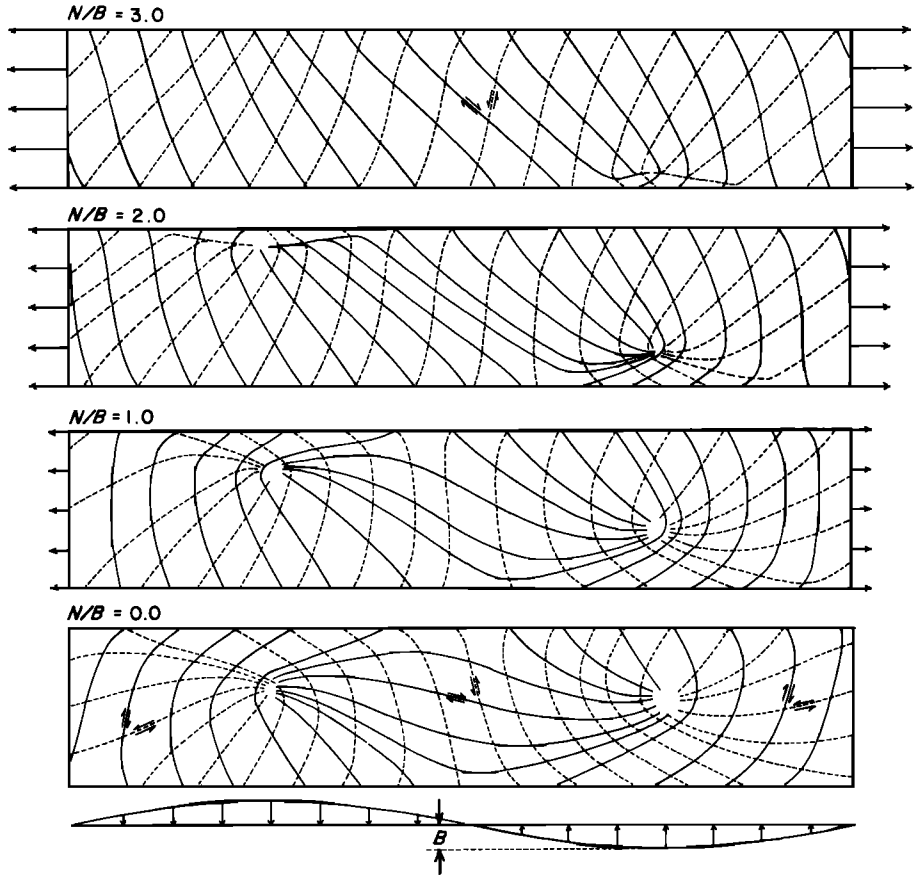

Fig. 3. Failure-surface trajectories, oriented at 30° to the maximum compressive stress, for different ratios of end normal extensional stress and sinusoidally varying base normal stress. Base normal stress of maximum magnitude B is constant in all four cross sections; end normal extensional stress N varies from zero in the lowermost cross section to 3 times the maximum base normal stress in the uppermost cross section. Solid lines represent clockwise shear; dashed lines represent anticlockwise shear.

horizontal extensional stress will elevate stresses until failure occurs.

Solitary Top and Base Normal Stress

Solitary top normal and base normal loads, forming a single pair with maximum loads horizontally separated, are intended to simulate possible stress conditions following thrusting (Figure 6). In such a configuration, surface relief is produced where the thin, tapered end of the hanging-wall block, with low flexural strength, is thrust over a thick footwall block of high flexural strength. In the root zone of such a thrust, a downward projecting bulge on the Moho may develop due to telescoping at deep crustal levels, especially if the ratio of crustal flexural strength to mantle-lithosphere flexural strength is high. Failure-surface trajectories and shear stress magnitudes between intermediate-depth points of zero shear stress (Figure 6) are virtually identical to those for a sinusoidally varying base normal stress (Figures 3 and 4), and the same inferences and

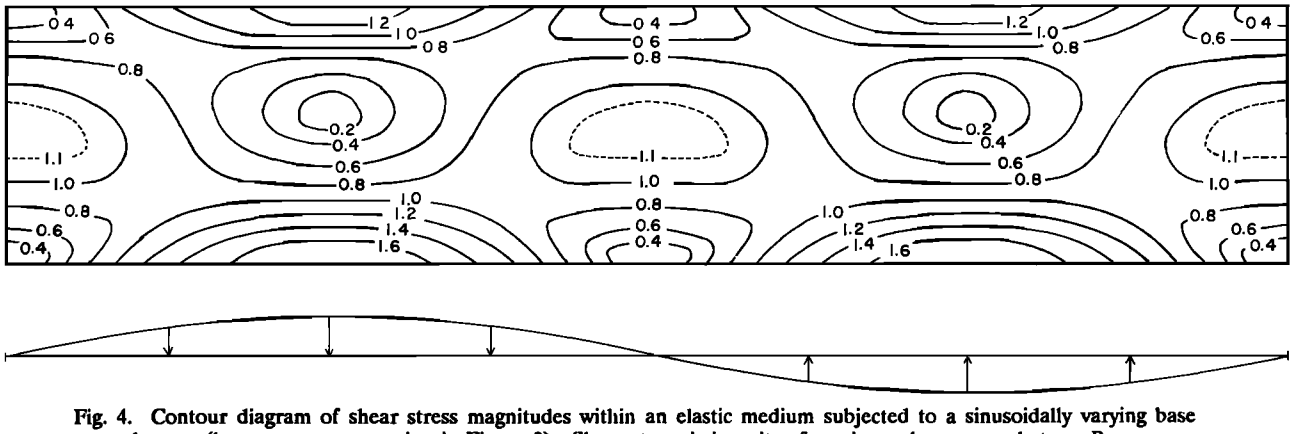

Fig. 4. Contour diagram of shear stress magnitudes within an elastic medium subjected to a sinusoidally varying base normal stress (lowermost cross section in Figure 3). Shear stress is in units of maximum base normal stress B.

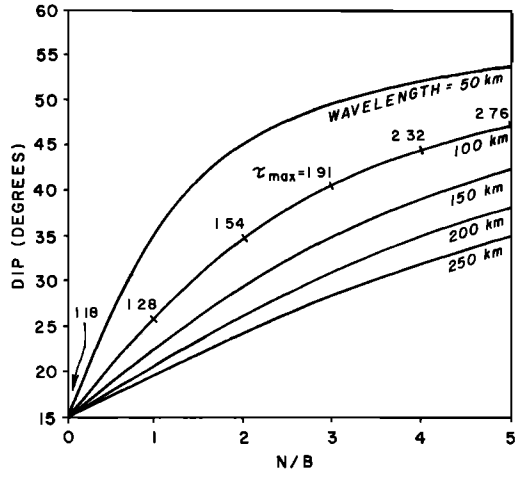

Fig. 5. Diagram showing stress conditions at the intermediate-depth points of maximum shear stress during pure sinusoidal flexure. Increasing the end normal extensional stress (N) and holding the flexural stress (B) constant result in progressive steepening of failure-surface trajectories asymptotically toward 60°. The five curves shown represent five different wavelengths of flexure. Increasing wavelength while holding amplitude (B) constant results in greater flexural stresses and a greater required extensional stress to cause the same increase in failure-surface dip. Also shown are shear stress magnitudes at points along the curve for a 100-km wavelength of sinusoidal flexure.

implications are applicable. Note that predicted low-angle normal failure surfaces at intermediate depths dip in the same direction as the older thrust fault or faults. Sufficient flexural strength in the mantle lithosphere will suppress development of a sharp Moho bulge, resulting in a broader, lower amplitude bulge. However, resultant failure-surface trajectories are not significantly different than those for a sharp Moho bulge.

In another possible tectonic setting, erosion at the Earth's surface could have largely removed topographic features originally associated with, or even compensated by, Moho relief. The resultant solitary Moho bump would exert an upward directed isostatic force balanced perhaps by much larger wavelength, lower amplitude surface relief. We model this tectonic configuration with a narrow, high-amplitude, downward protruding, Gaussian-shaped bump on the Moho overlain at the Earth's surface by a broad, low-amplitude Gaussian-shaped bump. Resultant stresses with and without end-normal stresses are shown in Figures 7 and 8. Listric normal failure-surface trajectories flatten downward and merge into a subhorizontal zone of coalescing trajectories (Figure 7) that correspond to a region of low to moderate shear stress (Figure 8). Shear stresses are of moderate magnitude in this zone between approximately 10 and 40 km horizontally from the point of maximum base normal stress. The inclination, depth, and shear stress magnitude of the zone of coalescing failure surfaces all increase with increasing extensional stress.

Stresses resulting from another possible tectonic configuration are illustrated by observing Figures 7 and 8 upside down. In this setting, a high-relief mountain range is isostatically compensated by a low-amplitude, long-wavelength, downward protruding Moho bulge. At large stress magnitudes, thrust faulting is predicted at shallow levels in the vicinity of the mountain range. At sufficient distance from the mountain range, gently dipping normal failure surfaces dip inward toward the axis of the mountain range, flatten at intermediate depths, and steepen downward toward the base of the cross section.

Application of these flexural stress models to environments of low-angle normal faulting requires an explanation for the preponderance of low-angle normal faults over the conjugate set of high-angle reverse faults. Subhorizontal foliation and associated zones of weakness may have localized initial failure surfaces. In any case, kinematic compatibility with the extensional regime causes the normal fault set to be activated preferentially to the reverse set when motion becomes finite.

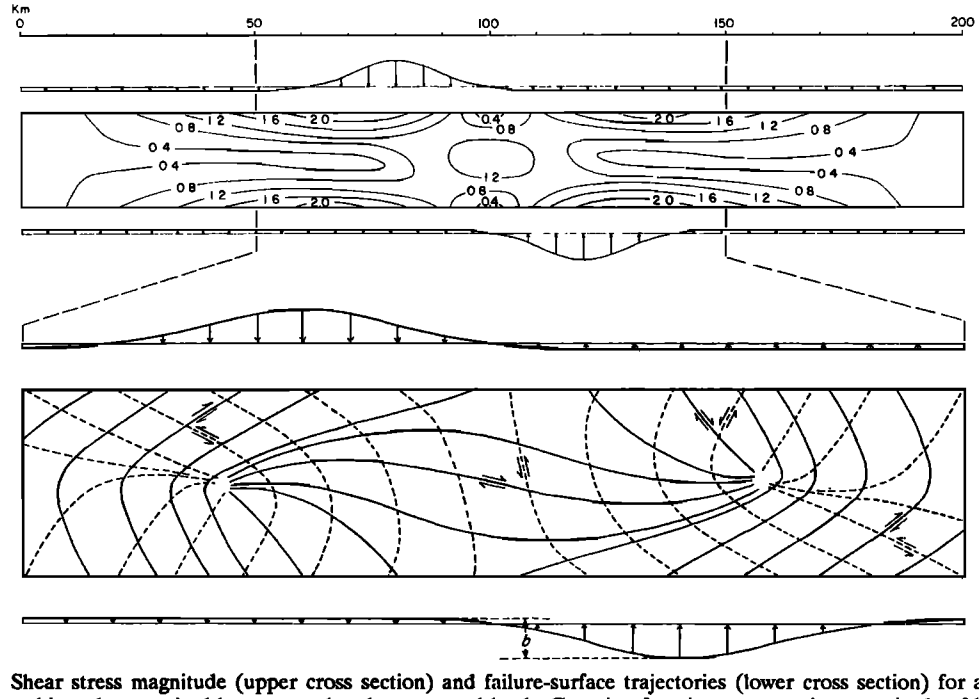

Fig. 6. Shear stress magnitude (upper cross section) and failure-surface trajectories (lower cross section) for an elastic medium subjected to a paired base normal and top normal load. Gaussian function representing magnitude of boundary normal stresses has a standard deviation of 10 km and unit amplitude (b). Shear stress magnitude is in units of maximum Gaussian function amplitude b.

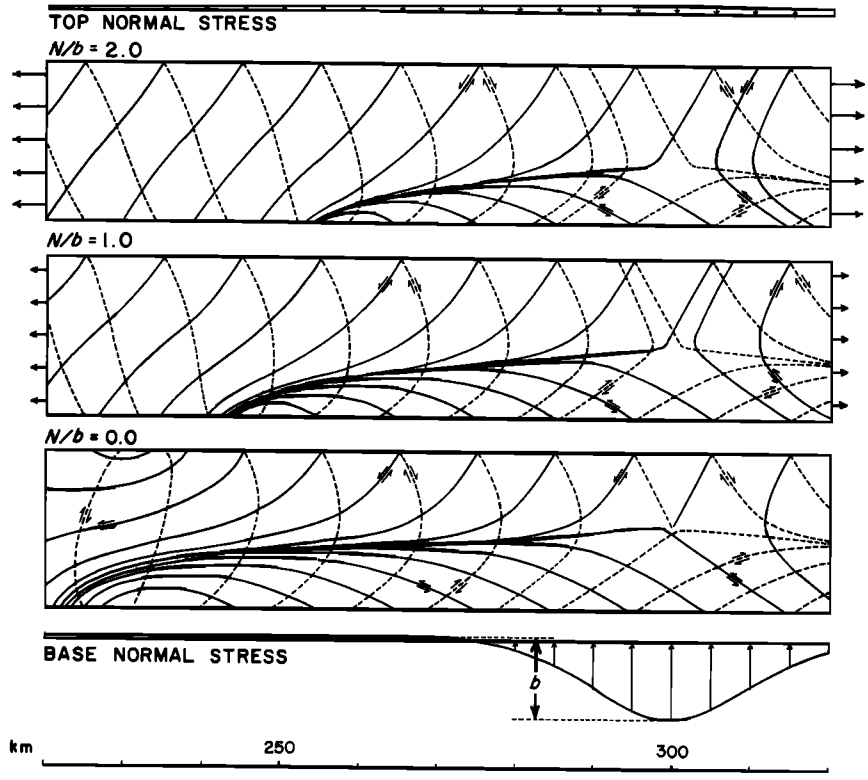

Fig. 7. Failure-surface trajectory diagrams for a solitary base normal load balanced by a solitary top normal load. Both loads have a Gaussian stress magnitude distribution and are centered within the 600-km cross section representing the fundamental wavelength of the Fourier series approximation. The lower stress magnitude function has a standard deviation of 10 and unit maximum amplitude (b). The upper stress magnitude function has a standard deviation of 100 and a maximum amplitude of $0.293b$. The maximum amplitude of the upper stress magnitude function was set at a value that would result in zero bending stress at the ends of the modeled 600-km-long cross section. Increasing end normal extensional stress results in generally greater dips of normal failure-surface trajectories.

Implications for the Basin and Range Province

Mesozoic to earliest Cenozoic crustal shortening in western North America produced relief on the Earth's surface and on the Moho. There is little doubt that a broad zone of crustal thickening and a corresponding regional downward bulge on the Moho developed in response to dominantly Mesozoic crustal shortening [e.g., *Wernicke et al.*, 1982; *Coney and Harms*, 1984]. The past existence of shorter wavelength Moho bulges is less well established. A shorter wavelength bulge associated with the east-west trending Maria fold and thrust belt in west-central Arizona and southeastern California [*Reynolds et al.*, 1986] is inferred to have influenced the geometry of Cenozoic low-angle normal faults and the magnitude of footwall uplift [*Spencer and Reynolds*, 1986, 1987]. This bulge is no longer present [*McCarthy et al.*, 1987; *Hauser et al.*, 1987] presumably as a result of crustal thinning and differential isostatic uplift. A short-wavelength Moho bulge detected by seismic refraction profiling is associated with the 2000- to 3000-m-high Catalina-Rincon metamorphic core complex in southeastern Arizona [*Holt et al.*, 1986; *Wallace et al.*, 1986]. In both of these areas, flexurally suppressed, isostatically uncompensated, downward protruding Moho bulges are inferred to have provided the driving force for uplift of the footwalls of Cenozoic low-angle normal faults following a decrease in the flexural strength of the lithosphere.

Our numerical simulations indicate that stresses produced by flexurally suppressed Moho bulges, and by uncompensated surface relief, are possible causes for low-angle normal fault initiation. Geologic examples of low-angle normal faults that possibly initiated as a result of stresses associated with a paired topographic load and Moho bulge, and that dip in the same direction as older thrust faults, include (1) west-central Arizona [*Spencer and Reynolds*, 1986, 1987], (2) the Death Valley region of southeastern California [*Wright and Troxel*, 1973, *Burchfiel and Davis*, 1981; *Burchfiel et al.*, 1983; *Stewart*, 1983; *Hodges et al.*, 1987], (3) southern Nevada [*Guth*, 1981; *Wernicke et al.*, 1985], and (4) west-central Utah [*Allmendinger et al.*, 1983]. Examples of low-angle normal faults that possibly initiated as a result of stresses associated with a solitary Moho bulge, and that dip outward from a central axis, include [see also *Wust*, 1986] (1) southeastern Arizona [*Davis and Hardy*, 1981; *Lingrey*, 1981; *Dickinson et al.*, 1987], (2) northwestern Utah and adjacent parts of southern Idaho [*Compton et al.*, 1977; *Saltzer and Hodges*, 1988; *Malavielle*, 1987], and (3) north-central Washington [*Cheney*, 1980; *Rhodes and Cheney*, 1981; *Tempelman-Kluit and Parkinson*, 1986].

The flexural strength of the mantle lithosphere must be the primary support of isostatically uncompensated Moho relief, as the lower crust is probably too weak [*Bird*, 1987]. Increased temperatures due to magmatism and associated decreased flexural strength of the mantle lithosphere would lead to increased upward directed, laterally varying normal stress on the strong upper crust. The resurgence of mid-Cenozoic magmatism is associated with low-angle normal fault initiation in the Basin and Range Province [*Coney*, 1980]. This relationship would be expected if heat associated with magmatism reduced the flexural strength of the mantle lithosphere, causing isostatically uncompensated Moho bulges to rise and transferring flexural stresses to the upper crust. We thus view the resurgence of magmatism as a possible trigger for increased flexural stress in

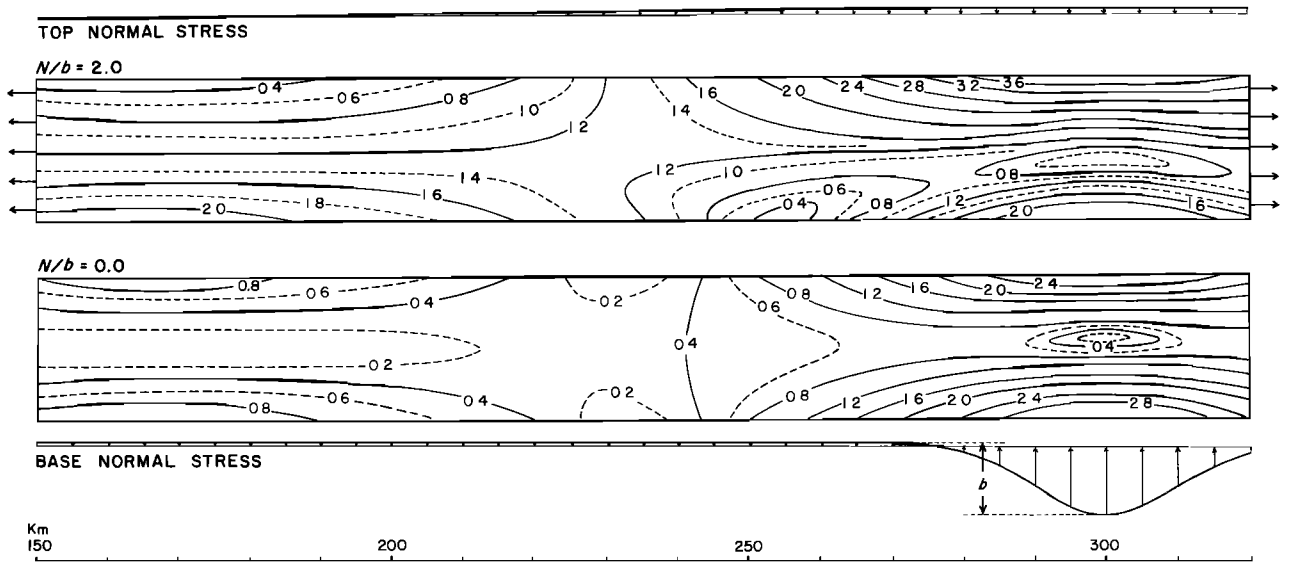

Fig. 8. Contour diagram of shear stress magnitude in units of maximum base normal stress (b) for the upper and lower cross sections in Figure 7. Listric normal-failure surfaces (Figure 7) flatten downward into a detachment zone with moderate stress amplitudes between approximately 265 and 290 km on the horizontal scale at the bottom of the figure.

the upper crust and resultant initiation of primary low-angle normal faults.

Dominantly mid-Cenozoic low-angle normal faulting in the Basin and Range Province generally preceded dominantly late Cenozoic high-angle normal faulting [*Zoback et al.*, 1981]. Our analysis suggests that reduction or elimination of flexural stresses in the upper crust resulted in a change in structural styles to more steeply dipping normal faults. Such a reduction could have had two causes: (1) flattening of the Moho by differential isostatic rebound and lower crustal ductile flow while the mantle lithosphere is hot and weak, and (2) later increased strength of the mantle lithosphere as a consequence of Moho uplift and cooling [*England*, 1983]. In addition, areas with high initial flexural stresses are predicted to have failed early, whereas areas with low initial flexural stress should have failed later as both horizontal extensional stresses and failure-surface dips increased (Figures 3, 5 and 7).

CONCLUSION

Airy stress functions are used to calculate stress conditions in an elastic, two-dimensional medium subjected to horizontal extensional stresses and laterally varying, vertically directed normal stresses. Results of such modeling are intended to approximate conditions in the strong upper crust where substantial stresses are accommodated by elastic strain prior to shear zone initiation. Stress trajectory diagrams reveal conjugate sets of predicted shear failure surfaces. Gently dipping shear failure surfaces, with a normal sense of shear, develop at intermediate depths in an elastic medium if the ratio of bending stress to horizontal extensional stress is sufficiently great. The general mechanics of flexure in an extensional tectonic setting are illustrated by modeling a sinusoidally varying, vertically directed normal stress with and without a horizontal extensional stress.

We model two specific tectonic configurations that produce stress conditions appropriate for low-angle normal fault initiation: (1) a paired topographic load and Moho bulge, and (2) a solitary, local Moho bulge compensated by regional topography. Thrust faulting is the most likely cause of such tectonic configurations prior to extensional tectonism in the Basin and Range Province. Isostatic consequences of laterally varying extensional tectonism, magmatism, erosion, and sedimentation are other possible causes, especially during later extensional tectonism. Application of our simulations to the Basin and Range Province suggests that the diverse regional dip directions of large, low-angle normal faults result from complex patterns of earlier crustal thickening and associated flexural stresses, and perhaps also from tectonic processes associated with extensional tectonism that produce new flexural stresses.

Acknowledgments. We thank An Yin for inspiring this work with discussions and a preprint prior to publication. We also thank An Yin and Brian Wernicke for reviews of an earlier manuscript that led to some revisions.

REFERENCES

Allmendinger, R. W., J. W. Sharp, D. Von Tish, L. Serpa, L. Brown, J. Oliver, and R. B. Smith, Cenozoic and Mesozoic structure of the eastern Basin and Range province, Utah, from COCORP seismic reflection data, *Geology, 11*, 532–536, 1983.

Bird, P., and D. Kemp, Nonlinear diffusion of crustal thickness and topography, *Eos Trans. AGU, 68*, 1465, 1987.

Brace, W. F., and D. L. Kohlstedt, Limits on lithospheric stress imposed by laboratory experiments, *J. Geophys. Res., 85*, 6248–6252, 1980.

Brune, J. N., T. L. Henyey, and R. F. Roy, Heat flow, stress, and rate of slip along the San Andreas fault, California, *J. Geophys. Res., 74*, 3821–3827, 1969.

Bryant, B., Lower plate rocks of the Buckskin Mountains, Arizona: A progress report, in Spencer, J. E., and S. J. Reynolds, eds., Geology and mineral resources of the Buckskin and Rawhide Mountains, west-central Arizona, *Ariz. Bur. Geol. Min. Tech. Bull., 198*, in press, 1988.

Burchfiel, B. C., and G. A. Davis, Mojave desert and environs, in *The Geotectonic Development of California*, edited by W. G. Ernst, pp. 217–252, Prentice-Hall, Englewood Cliffs, N. J., 1981.

Burchfiel, B. C., D. Walker, G. A. Davis, and B. Wernicke, Kingston Range and related detachment faults–a major "breakaway" zone in the southern Great Basin, *Geol. Soc. Am. Abstr. Programs., 15*, 536, 1983.

Byerlee, J., Friction of rocks, *Pure Appl. Geophys., 116*, 615–626, 1978.

Chen, W.-P., and P. Molnar, Focal depths of intracontinental and intraplate earthquakes and their implications for the thermal and mechanical properties of the lithosphere, *J. Geophys. Res., 88*, 4183–4214, 1983.

Cheney, E. S., Kettle Dome and related structures of northeastern

Washington, Cordilleran Metamorphic Core Complexes, *Mem. Geol. Soc. Am. 153*, 463–484, 1980.

Compton, R. R., V. R. Todd, R. E. Zartman, and C. W. Naeser, Oligocene and Miocene metamorphism, folding, and low-angle faulting in northwestern Utah, *Geol. Soc. Am. Bull., 88*, 1237–1250, 1977.

Coney, P. J., Cordilleran metamorphic core complexes–An overview, Cordilleran Metamorphic Core Complexes, *Mem. Geol. Soc. Amer. 153*, 7–31, 1980.

Coney, P. J., and T. A. Harms, Cordilleran metamorphic core complexes: Cenozoic extensional relics of Mesozoic com-pression, *Geology, 12*, 550–554, 1984.

Crittenden, M. D., Jr., P. J. Coney, and G. H. Davis (Eds.), Cordilleran Metamorphic Core Complexes, *Mem. Geol. Soc. Am. 153*, 1980.

Davis, G. A., J. L. Anderson, E. G. Frost, and T. J. Shackelford, Mylonitization and detachment faulting in the Whipple-Buckskin-Rawhide Mountains terrane, southeastern California and western Arizona, Cordilleran Metamorphic Core Complexes, Mem. *Geol. Soc. Am. 153*, 79–129, 1980.

Davis, G. A., G. S. Lister, and S. J. Reynolds, Structural evolution of the Whipple and South Mountains shear zones, southwestern United States, *Geology, 14*, 7–10, 1986.

Davis, G. H., Shear-zone model for the origin of metamorphic core complexes, *Geology, 11*, 342–347, 1983.

Davis, G. H., and J. J. Hardy, Jr., The Eagle Pass detachment, southeastern Arizona: Product of mid–Miocene listric (?) normal faulting in the southern Basin and Range, *Geol. Soc. Am. Bull., 92*, 749–762, 1981.

De Rito, R. F., F. A. Cozzarelli, and Hodge, A forward approach to the problem of nonlinear viscoelasticity and the thickness of the mechanical lithosphere, *J. Geophys. Res., 91*, 8295–8313, 1986.

Dickinson, W. R., T. C. Goodlin, J. A. Grover, R. A. Mark, and M. Shafiqullah, Low-angle normal-fault system along the range front of the southwestern Galiuro Mountains in southeastern Arizona, *Geology, 15*, 727–730, 1987.

England, P., Constraints on extension of continental lithosphere, *J. Geophys. Res., 88*, 1145–1152, 1983.

Frost, E. G., and D. L. Martin (Eds.), *Mesozoic-Cenozoic Tectonic Evolution of the Colorado River Region, California, Arizona, and Nevada*, Cordilleran Publishers, San Diego, Calif., 1982.

Frost, E. G., and D. A. Okaya, Application of seismic reflection profiles to tectonic analysis in mineral exploration, Frontiers in Geology and Ore Deposits of Arizona and the Southwest, *Ariz. Geol. Soc. Dig., 16*, 137–152, 1986.

Guth, P. L., Tertiary extension north of the Las Vegas shear zone, Sheep and Desert Ranges, Clark County, Nevada, *Geol. Soc. Am. Bull., 92*, 763–771, 1981.

Hafner, W., Stress distributions and faulting, *Geol. Soc. Am. Bull., 62*, 373–398, 1951.

Hanks, T. C., Earthquake stress drops, ambient tectonic stresses and stresses that drive plate motions, *Pure Appl. Geophys., 115*, 441–458, 1977.

Hauser, E. C., J. Gephart, T. Latham, J. Oliver, S. Kaufman, L. Brown, and I. Lucchitta, COCORP Arizona transect: Strong crustal reflections and offset Moho beneath the transition zone, *Geology, 15*, 1103–1106, 1987.

Hodges, K. V., J. D. Walker, and B. P. Wernicke, Footwall structural evolution of the Tucki Mountain detachment system, Death Valley region, southeastern California, Continental extensional tectonics, *Spec. Publ. Geol. Soc. London, 28*, 393–408, 1987.

Holt, W. E., C. G. Chase, and T. C. Wallace, Crustal structure from three-dimensional gravity modeling of a metamorphic core complex: A model for uplift, Santa Catalina-Rincon Mountains, Arizona, *Geology, 14*, 927–930, 1986.

Howard, K. A., P. Stone, M. A. Pernokas, and R. F. Marvin, Geologic and geochronologic reconnaissance of the Turtle Mountains area, California: West border of the Whipple detachment terrane, in *Mesozoic-Cenozoic Tectonic Evolution of the Colorado River Region, California, Arizona, and Nevada*, edited by E. G. Frost and D. L. Martin, pp. 341–354, Cordilleran Publishers, San Diego, Calif., 1982.

Jackson, J. A., Active normal faulting and crustal extension, Continental extensional tectonics, *Spec. Publ. Geol. Soc. London, 28*, 3–17, 1987.

Jeffreys, H., *The Earth*, 6th ed., Cambridge University Press, Cambridge, 1976.

John, B. E., Geometry and evolution of a mid–crustal extensional fault system: Chemehuevi Mountains, southeastern California, Continental extensional tectonics, *Spec. Publ. Geol. Soc. London, 28*, 313–335, 1987.

Kirby, S. H., and A.K. Kronenberg, Rheology of the lithosphere: Selected topics, Contributions in tectonophysics, U.S. National Report to International Union of Geodesy and Geophysics 1983–1986, *Rev. Geophys., 25*, 1219–1244, 1987.

Lachenbruch, A. H., J. H. and Sass, Heat flow and energetics of the San Andreas fault zone, *J. Geophys. Res., 85*, 6185–6222, 1980.

Lingrey, S., Older-over-younger gravity sliding in the eastern Rincon Mountains, Catalina-Rincon metamorphic core complex, Arizona, *Geol. Soc. Am. Abstr. Programs, 13*, 67, 1981.

Malavielle, J., Extensional shearing deformation and kilometer–scale "a" type folds in a Cordilleran metamorphic core complex, *Tectonics, 6*, 423–432, 1987.

McCarthy, J., G. S. Fuis, and J. Wilson, Crustal structure in the region of the Whipple Mountains metamorphic core complex, from seismic refraction results, *Geol. Soc. Am. Abstr. Programs, 19*, 763, 1987.

McNutt, M. K., and H. W. Menard, Constraints on yield strength in the oceanic lithosphere derived from observations of flexure, *Geophys. J. R. Astron. Soc., 71*, 363–394, 1982.

Miller, J. M. G., and B. E. John, Detached strata in a Tertiary low–angle normal fault terrane, southeastern California: A sedimentary record of unroofing, breaching, and continued slip, *Geology, 16*, 645–649, 1988.

Mount, V. S., and J. Suppe, State of stress near the San Andreas fault: Implications for wrench tectonics, *Geology, 15*, 1143–1146, 1987.

Raleigh, B., and J. Evernden, Case for low deviatoric stress in the lithosphere, *Mechanical Behavior of Crustal Rocks, Geophys. Mono. 24*, edited by N. L. Carter, pp. 173–186, AGU, Washington, D.C., 1981.

Rehrig, W. A., and S. J. Reynolds, Geologic and geochronologic reconnaissance of a northwest-trending zone of metamorphic core complexes in southern and western Arizona, Cordilleran Metamorphic Core Complexes, *Mem. Geol. Soc. Am. 153*, 131–157, 1980.

Reynolds, S. J., Geology of the South Mountains, central Arizona, *Ariz. Bur. Geol. Min. Tech. Bull., 195*, 1985.

Reynolds, S. J., and J. E. Spencer, Evidence for large-scale transport on the Bullard detachment fault, west-central Arizona, *Geology, 13*, 353–356, 1985.

Reynolds, S. J., J. E. Spencer, S. M. Richard, and S. E. Laubach, Mesozoic structures in west-central Arizona, Frontiers in Geology and Ore Deposits of Arizona and the Southwest, *Ariz. Geol. Soc. Dig., 16*, 35–51, 1986.

Rhodes, B. P., and E. S. Cheney, Low-angle faulting and the origin of Kettle dome, a metamorphic core complex in northeastern Washington, *Geology, 9*, 366–369, 1981.

Saltzer, S. D., and K. V. Hodges, The Middle Mountain shear zone, southern Idaho: Kinematic analysis of an early Tertiary high-temperature detachment, *Geol. Soc. Am. Bull., 100*, 96–103, 1988.

Sibson, R. H., Fault zone models, heat flow, and the depth distribution of earthquakes in the continental crust of the United States, *Bull. Seismol. Soc. Am., 72*, 151–163, 1982.

Spencer, J. E., Origin of folds of Tertiary low-angle fault surfaces, southeastern California and western California, *Mesozoic-Cenozoic Tectonic Evolution of the Colorado River Region, California, Arizona, and Nevada*, edited by E. G. Frost and D. L. Martin, pp. 123–134, Cordilleran Publishers, San Diego, Calif., 1982.

Spencer, J. E., Role of tectonic denudation in warping and uplift of low–angle normal faults, *Geology, 12*, 95–98, 1984.

Spencer, J. E., Miocene low-angle normal faulting and dike emplacement, Homer Mountain and surrounding areas, southeastern California and southernmost Nevada, *Geol. Soc. Am. Bull., 96*, 1140–1155, 1985.

Spencer, J. E., and S. J. Reynolds, Some aspects of the Middle Tertiary tectonics of Arizona and southeastern California, Frontiers in the Geology and Ore Deposits of Arizona and the Southwest, *Ariz. Geol. Soc. Dig., 16*, 102–107, 1986.

Spencer, J. E., and S. J. Reynolds, Interaction between Mesozoic and Cenozoic tectonic features in the Buckskin Mountains and adjacent areas, west-central Arizona and southeastern California, *Geol. Soc. Am. Abstr. Programs, 19*, 852, 1987.

Spencer, J. E., and S. J. Reynolds (Eds.), Geology and mineral resources of the Buckskin and Rawhide Mountains, west-central Arizona, *Ariz. Bur. Geol. Min. Tech. Bull., 198, in press*, 1988.

Stewart, J. H., Extensional tectonics in the Death Valley area, California: Transport of the Panamint Range structural block 80 km northwestward, *Geology, 11*, 153–157, 1983.

Tempelman-Kluit, D., and D. Parkinson, Extension across the Eocene Okanagon crustal shear in southern British Columbia, *Geology, 14*, 318–321, 1986.

Timoshenko, S. P., and J. N. Goodier, *Theory of Elasticity*, 3rd ed., McGraw-Hill, New York, 1970.

Wallace, T. C., C. G. Chase, W. E. Holt, and J. W. Hiller, A geophysical study of the crustal structure near a metamorphic core complex, Frontiers in Geology and Ore Deposits of Arizona and the Southwest, *Ariz. Geol. Soc. Dig.*, *16*, 153–158, 1986.

Wernicke, B., Low-angle faults in the Basin and Range Province–Nappe tectonics in an extending orogen, *Nature, 291*, 645–648, 1981.

Wernicke, B., J. E. Spencer, B. C. Burchfiel, and P. L. Guth, Magnitude of crustal extension in the southern Great Basin, *Geology, 10*, 499–502, 1982.

Wernicke, B., J. D. Walker, and M. S. Beaufait, Structural discordance between Neogene detachments and frontal Sevier thrusts, central Mormon Mountains, southern Nevada, *Tectonics, 4*, 213–246, 1985.

Wright, L. A., and B. W. Troxel, Shallow–fault interpretation of Basin and Range structure, southwestern Great Basin, in *Gravity and Tectonics*, edited by K. DeJong and R. Scholten, pp. 397–407, John Wiley, New York, 1973.

Wust, S. L., Regional correlation of extension directions in Cordilleran metamorphic core complexes, *Geology, 14*, 828–830, 1986.

Yin, A., Origin of regional, rooted low-angle normal faults: A mechanical model and its tectonic implications, *Eos Trans. AGU, 68*, 1449, 1987.

Zoback, M. D., M. L. Zoback, V. S. Mount, J. Suppe, J. P. Eaton, J. H. Healy, D. Oppenheimer, and others, New evidence on the state of stress of the San Andreas fault system, *Science, 238*, 1105–1111, 1987.

Zoback, M. L., R. E. Anderson, and G. A. Thompson, Cenozoic evolution of the state of stress and style of tectonism of the Basin and Range province of the western United States, *Philos. Trans. R. Soc. London, Ser. A, 300*, 189–216, 1981.

C. G. Chase, Department of Geosciences, University of Arizona, Tucson AZ 85721.

J. E. Spencer, Arizona Geological Survey, 845 North Park Avenue, Tucson, AZ 85719.

(Received February 10, 1988;
revised August 24, 1988;
accepted September 26, 1988.)